Generalized labeled multi-Bernoulli filter with kernel-based ensemble Gaussian mixture filtering for orbit determination with sparse data

Sehyun Yun
The University of Texas at Austin
Nicholas Ravago, Benjamin L. Reifler, Renato Zanetti, Brandon A. Jones
The University of Texas at Austin

ABSTRACT

The modified kernel-based ensemble Gaussian mixture filtering (EnGMF) has been recently proposed by Yun et al. [1] to obtain accurate and fast orbit determination capabilities under the sparse observation environment. As a continuation of the study, in this paper, the EnGMF is used in combination with the generalized labeled multi-Bernoulli (GLMB) multi-target tracking filter to track and identify multiple space objects. Moreover, the bi-fidelity propagation and an adaptive algorithm introduced in the previous study are also applied to the baseline algorithm (i.e., the GLMB with the ENGMF) to reduce computational burden with an acceptable loss in accuracy. Through numerical simulations, the performances of the proposed filters are evaluated and compared in terms of accuracy and computational speed.

1. INTRODUCTION

Space situational awareness (SSA) refers to the knowledge of the near-space environment, including the ability to track and predict the states of space objects (SOs) orbiting Earth and in cislunar space. The majority of SOs in Earth orbits are debris objects, such as used satellites and rocket fragments. As the space domain becomes more congested due to the launching of new objects, it poses a serious threat to newly launched satellites and the risk of collision between SOs considerably increases. A multi-target tracking algorithm is proposed for sparse-data tracking by using an efficient data association algorithm and an accurate and computationally efficient nonlinear estimation algorithm for orbit determination. In this study, the modified kernel-based ensemble Gaussian mixture filtering (EnGMF) [1] is used in combination with the generalized labeled multi-Bernoulli (GLMB) multi-target tracking filter [2] to track and identify multiple SOs.

The GLMB filter is designed to provide estimates of object trajectories based on the labeled random finite set (RFS) theory [2]. An RFS is a finite set containing a random number of random variables, and a labeled RFS includes a unique label on each element to indicate identity. The GLMB density is a type of labeled RFS density that provides an analytical solution to the Bayes multi-target filter recursion, and in the GLMB filter, the multi-target state and measurement set are modeled as RFSs. One of the challenges existing in the GLMB filter (and any hypothesis-based multi-target tracker) is high computational cost due to the exponential increase of the number of components in the filtering process; therefore, it requires a truncation strategy to remain computationally tractable [3]. To reduce the computational cost, in this work the EnGMF is used as the single-target filter to reduce the overall computational burden when compared to other state-of-the-art nonlinear estimators [1].

The EnGMF is developed to efficiently track SOs with short and sparse observation data (i.e., tracking passes are short and sparse) [1]. The EnGMF takes the benefits of both particle filter (PF) [4] and Gaussian sum filter (GSF) [5, 6]. The key idea of the algorithm is that the propagated particles of PF converted into Gaussian mixtures using kernel density estimation (KDE) [7]. In other words, each and every sample is considered as a Gaussian component with the same covariance (i.e., bandwidth) matrix. The bandwidth matrix can be selected by numerically solving an optimization problem; however, in this study, Silverman's rule of thumb [8] is employed to estimate the bandwidth matrix to reduce the KDE computational cost. When the sampling distribution is Gaussian, the optimal bandwidth matrix is obtained by Silverman's rule of thumb based on the mean integrated squared error (MISE) as a performance criterion. Moreover, in our previous work [1], we demonstrated that Silverman's rule will result in conservative (large)

estimates even though the sampling distribution is not close to Gaussian, which means inaccuracies make the estimator conservative rather than divergent.

In addition, a bi-fidelity approach to propagation and an adaptive algorithm are applied to the EnGMF to reduce its computational cost with an acceptable loss in accuracy. The bi-fidelity approach employs both low- and high-fidelity models to minimize computational cost for the propagation of the EnGMF, while maximizing the accuracy of orbit uncertainty propagation [9]. Choosing the appropriate number of particles is also one key parameter of the EnGMF to improve its computational complexity. Thus, an adaptive algorithm is employed to select an appropriate number of particles of the EnGMF based on the convergence assessment [10] using a predictive observation probability density function (PDF).

The remainder of this paper is organized as follows. First, the GLMB multi-target tracking filter is described. Then, the EnGMF developed for orbit determination with sparse observation data is introduced with the bi-fidelity propagation and an adaptive algorithm in Section 3. In Section 4, simulation results are shown using the proposed algorithms followed by some concluding remarks on the methodology and results.

2. GENERALIZED LABELED MULTI-BERNOULLI FILTER

The Bayes multi-target filter is a generalization of the single-target Bayes filter to estimate the trajectories of multiple targets and the GLMB provides an analytical solution to the Bayes multi-target filter recursion while maintaining target identity using a labeled RFS [2, 3]. The multi-target state $\boldsymbol{X}_k$ and observation Y_k are represented as a labeled RFS as follow:

$$\begin{aligned} \boldsymbol{X}_k &= \{\boldsymbol{x}_1, \boldsymbol{x}_2, \cdots, \boldsymbol{x}_{n_k}\} = \{(x_1, \ell_1), (x_2, \ell_2), \cdots, (x_{n_k}, \ell_{n_k})\} \subset \mathbb{X} \times \mathbb{L} \\ Y_k &= \{y_1, y_2, \cdots, y_{m_k}\} \subset \mathbb{Y} \end{aligned} \tag{1}$$

where $\mathbb{X}$ and $\mathbb{Y}$ are the single-target state and measurement spaces, respectively, $\mathbb{L}$ is a discrete label space, and n_k and m_k indicate the number of estimated states and observations, respectively, at time k. It is worth noting that n_k may not be equal to m_k due to clutter and missed detections. Each element $\boldsymbol{x}$ of the RFS $\boldsymbol{X}$ is composed of the estimated single-target state x and a distinct label ℓ of the state x. The observation RFS Y consists of multiple measurement vectors y scanned with a singe sensor. The GLMB filter then predicts and updates the multi-target density $\boldsymbol{\pi}(\boldsymbol{X})$. To derive an analytical solution to the Bayes multi-target filter, the formulation of $\boldsymbol{\pi}(\boldsymbol{X})$ is described in the remainder of this section.

Let $\mathcal{L} : \mathbb{X} \times \mathbb{L} \to \mathbb{L}$ be the projection $\mathcal{L}(x, \ell) = \ell$ from labeled RFSs to labels, then each possible target has a unique label if and only if a finite subset set $\boldsymbol{X}$ of $\mathbb{X} \times \mathbb{L}$ and its labels $\mathcal{L}(\boldsymbol{X}) = \{\mathcal{L}(\boldsymbol{x}) : \boldsymbol{x} \in \boldsymbol{X}\}$ have the same cardinality, i.e., $\delta_{|\boldsymbol{X}|}(|\mathcal{L}(\boldsymbol{X})|) = 1$ where

$$\delta_A(B) \equiv \begin{cases} 1 & \text{if } B = A \\ 0 & \text{otherwise} \end{cases} \tag{2}$$

is a generalized delta function that supports sets and vectors. For simple notation,

$$\Delta(\boldsymbol{X}) \triangleq \delta_{|\boldsymbol{X}|}(|\mathcal{L}(\boldsymbol{X})|) \tag{3}$$

denotes a distinct label indicator, and let the function $\mathcal{F}$ denote the set of all finite subsets of a space.

A labeled multi-Bernoulli (LMB) RFS is parameterized by $\left\{\left(r^{(\ell)}, p^{(\ell)}\right)\right\}_{\ell \in \mathbb{L}}$, where $r^{(\ell)}$ is the probability that target ℓ exists and $p^{(\ell)}$ is its state-space PDF. The PDF of the LMB RFS is then described as follows:

$$\boldsymbol{\pi}(\boldsymbol{X}) = \Delta(\boldsymbol{X}) w(\mathcal{L}(\boldsymbol{X})) p^{\boldsymbol{X}} \tag{4}$$

where the multi-object exponential is

$$p^{\boldsymbol{X}} \equiv \prod_{\boldsymbol{x} \in \boldsymbol{X}} p(\boldsymbol{x}) \tag{5}$$

and

$$w(L) = \prod_{i \in \mathbb{L}} \left(1 - r^{(i)}\right) \prod_{\ell \in L} \frac{1_{\mathbb{L}}(\ell) r^{(\ell)}}{1 - r^{(\ell)}} \tag{6}$$

$$p(x, \ell) = p^{(\ell)}(x) \tag{7}$$

$$1_A(B) \equiv \begin{cases} 1 & \text{if } B \subseteq A \\ 0 & \text{otherwise} \end{cases} \tag{8}$$

A GLMB density can be written as a mixture of multi-target exponentials based on the LMB density as follows:

$$\boldsymbol{\pi}(\boldsymbol{X}) = \Delta(\boldsymbol{X}) \sum_{c \in \mathbb{C}} w^{(c)}(\mathcal{L}(\boldsymbol{X})) \left[p^{(c)}\right]^{\boldsymbol{X}} \tag{9}$$

where $\mathbb{C}$ is an index set that allows for multiple possible realizations for a set of target labels, each $p^{(c)}$ is a PDF, and the weights must satisfy

$$\sum_{L \subseteq \mathbb{L}} \sum_{c \in \mathbb{C}} w^{(c)}(L) = 1 \tag{10}$$

An alternative formulation known as a δ-GLMB RFS is used for the GLMB filter in this work, which can be characterized by a set of components $(I, \xi^H) \in \mathcal{F}(\mathbb{L}) \times \Xi^H$, with associated weights $w^{(I,\xi^H)} = w^{(\xi^H)}(I)$. The function $\mathcal{F}(\mathbb{L})$ represents the set of all finite subsets of $\mathbb{L}$ and a space Ξ^H represents the history of measurement associations to a given track. Therefore, the components (I, ξ^H) can be interpreted as the data association hypotheses with $w^{(I,\xi^H)}$ being the probability that the hypothesis is true. The δ-GLMB density is expressed as follows:

$$\boldsymbol{\pi}(\boldsymbol{X}) = \Delta(\boldsymbol{X}) \sum_{(I,\xi^H) \in \mathcal{F}(\mathbb{L}) \times \Xi^H} w^{(I,\xi^H)} \delta_I(\mathcal{L}(\boldsymbol{X})) \left[p^{(\xi^H)}\right]^{\boldsymbol{X}} \tag{11}$$

Reference [2] shows that the δ-GLMB RFS is conjugate with respect to the multi-object likelihood function as well as being closed under the multi-object Chapman-Kolmogorov equation with respect to the multi-object transition kernel; that is, it presents that the δ-GLMB RFS provides a closed-form solution to the Bayes multi-target filter.

The space of labels corresponding to objects that may be spontaneously born at the following timestep is denoted $\mathbb{B}_+$, resulting in the predicted label space $\mathbb{L}_+ = \mathbb{L} \cup \mathbb{B}_+$. Let Θ_+ be the set of one-to-one maps $\theta_+(l) : \mathbb{L}_+ \to \{0, \ldots, |Z_+|\}$ assigning measurements at the following timestep to object labels, with $\theta_+(l) = 0$ indicating that no measurement is assigned to the object with label l at that time. Given the δ-GLMB density in Eq. (11), the predicted and updated density at the following timestep is

$$\boldsymbol{\pi}_+(\boldsymbol{X}_+) \propto \Delta(\boldsymbol{X}_+) \sum_{I, \xi^H, I_+, \theta_+} w^{(I,\xi^H)} w^{(I,\xi^H,I_+,\theta_+)}(Z_+) \delta_{I_+}(\mathcal{L}(\boldsymbol{X}_+)) \left[p_+^{(\xi^H,\theta_+)}(\cdot \mid Z_+)\right]^{\boldsymbol{X}_+} \tag{12}$$

where $I \in \mathcal{F}(\mathbb{L})$, $\xi^H \in \Xi^H$, $I_+ \in \mathcal{F}(\mathbb{L}_+)$, $\theta_+ \in \Theta_+$, and

$$w^{(I,\xi^H,I_+,\theta_+)}(Z_+) = (r_{B,+})^{\mathbb{B}_+ \cap I_+} (1 - r_{B,+})^{\mathbb{B}_+ - I_+} \left(\bar{p}_S^{(\xi^H)}\right)^{I \cap I_+} \left(1 - \bar{p}_S^{(\xi^H)}\right)^{I - I_+} \left(\bar{\psi}_+^{(\xi^H,\theta_+)}(\cdot \mid Z_+)\right)^{I_+} \tag{13}$$

$$p_+^{(\xi^H,\theta_+)}(x_+, l \mid Z_+) = \frac{\bar{p}_+^{(\xi^H)}(x_+, l) \psi_+^{(\theta_+(l))}(x_+, l \mid Z_+)}{\bar{\psi}_+^{(\xi^H,\theta_+(l))}(l \mid Z_+)} \tag{14}$$

$$\bar{p}_+^{(\xi^H)}(x_+, l) = 1_{\mathbb{B}_+}(l) p_{B,+}(x_+, l) + 1_{\mathbb{L}}(l) \frac{\left\langle p_S(\cdot, l) f_{S,+}(x_+ \mid \cdot, l), p^{(\xi^H)}(\cdot, l) \right\rangle}{\bar{p}_S^{(\xi^H)}(l)} \tag{15}$$

$$\bar{p}_S^{(\xi^H)}(l) = \left\langle p_S(\cdot, l), p^{(\xi^H)}(\cdot, l) \right\rangle \tag{16}$$

$$\bar{\psi}_+^{(\xi^H,i)}(l \mid Z_+) = \left\langle \bar{p}_+^{(\xi^H)}(\cdot, l), \psi_+^{(i)}(\cdot, l \mid Z_+) \right\rangle \tag{17}$$

$$\psi_+^{(i)}(x_+, l \mid Z_+) = \delta_0(i)(1 - p_D(x_+, l)) + (1 - \delta_0(i)) \frac{p_D(x_+, l) g(z_{+,i} \mid x_+, l)}{\kappa(z_{+,i})} \tag{18}$$

where $r_{B,+}(l)$ is the probability that object l is born, $p_{B,+}$ is the single-target probability density for the newborn object, p_S is the probability of survival from one step to the next, p_D is the probability of detection, $f_{S,+}$ is the surviving object transition density, g is the measurement likelihood, and κ is the assumed clutter intensity.

The δ-GLMB filtering density is truncated by constructing a cost matrix for each prior component (I,ξ^H) and using a ranked assignment algorithm to generate only those posterior components that have the highest weights [11]. The cost of the single association hypothesis i for object l, where $i<0$ indicates that the object does not exist, $i=0$ indicates that it exists but was not detected, and $i>0$ indicates that it exists and generated measurement $z_{+,i}$, is $-\log\left(\eta^{(I,\xi^H)}(l,i)\right)$, where

$$\eta^{(I,\xi^H)}(l,i)=\begin{cases}1-r_{B,+}(l), & i<0\wedge l\in\mathbb{B}_+\\ r_{B,+}(l)\bar{\psi}_+^{(\xi^H,i)}(l\mid Z_+), & i\geq 0\wedge l\in\mathbb{B}_+\\ 1-\bar{p}_S^{(\xi^H)}(l), & i<0\wedge l\in I\\ \bar{p}_S^{(\xi^H)}(l)\bar{\psi}_+^{(\xi^H,i)}(l\mid Z_+), & i\geq 0\wedge l\in I\end{cases} \tag{19}$$

such that the total cost of a given assignment vector is directly related to its weight.

3. MODIFIED KERNEL-BASED ENSEMBLE GAUSSIAN MIXTURE FILTERING

The EnGMF has been recently proposed by Yun et al. [1] to efficiently track SOs with short and sparse observation data (i.e., tracking passes are short and sparse). As a single-target nonlinear filter, the EnGMF algorithm is briefly introduced in this section and the details of the algorithm are explained in [1].

As a recursive algorithm, the knowledge of the distribution $p(x_{k-1}|y_{k-1})$ at the prior time is assumed and approximated by N independent and identically distributed (i.i.d.) samples $x_{k-1}^{(i)}$ such that

$$p(x_{k-1}|y_{k-1})\approx\sum_{i=1}^{N}\frac{1}{N}\delta(x_{k-1}-x_{k-1}^{(i)}) \tag{20}$$

where $\delta(\cdot)$ is the Dirac delta function. As in the bootstrap particle filter (BPF) [4], in the time update step, a set of samples at the next time step is generated using the Markov transition kernel $p(x_k|x_{k-1})$. The Markov kernel represents the dynamics of a system and it is assumed in this work that all estimators use the true dynamic model without process noise.

The propagated samples are then converted into Gaussian mixtures using kernel density estimation (KDE). In other words, each and every sample is considered as a Gaussian component with the same covariance (i.e., bandwidth) matrix. The approximated GMM of the propagated samples is expressed as follows:

$$p(x_k)\approx\sum_{i=1}^{N}\frac{1}{N}n(x_k;x_{k|k-1}^{(i)},B) \tag{21}$$

where the bandwidth matrix B can be calculated by [12]

$$B=\beta\hat{P}_{k|k-1} \tag{22}$$

where β is the bandwidth parameter, $0\leq\beta\leq 1$, and $\hat{P}_{k|k-1}$ is the sample covariance matrix calculated from the propagated samples. The means of Gaussian components are obtained from each particle $\boldsymbol{x}_{k|k-1}^{(i)}$ and all GMM weights are equal to $1/N$. The bandwidth matrix can be selected by numerically solving an optimization problem; however, in this study, to reduce the KDE computational cost, Silverman's rule of thumb [8] is employed to estimate the bandwidth matrix B_S as follows:

$$B_S=\beta_S\hat{P}_{k|k-1}=h_S\left(\frac{4}{n_x+2}\right)^{\frac{2}{n_x+4}}N^{-\frac{2}{n_x+4}}\hat{P}_{k|k-1} \tag{23}$$

where h_S is a tuning parameter and $n_{\boldsymbol{x}}$ is the dimension of the state. When the sampling distribution is Gaussian and $h_s=1$, the optimal bandwidth matrix is obtained by Silverman's rule of thumb based on the mean integrated squared error (MISE) as a performance criterion. Therefore, in this study, the equinoctial orbital elements [13] are used instead

of Cartesian coordinates to make the SO dynamics nearly linear. Moreover, in our previous work [1], we demonstrated that Silverman's rule will result in conservative (large) estimates even though the sampling distribution is not close to Gaussian, which means inaccuracies make the estimator conservative rather than divergent. In addition, the tuning parameter, $h_S \leq 1$, can be tuned according to a system to improve the filter's performance.

Finally, the measurement information is incorporated by updating the means, covariance matrices, and the weights of all N Gaussian components in the same way as the measurement update of the GSF. In the measurement update step, each Gaussian component may be updated using the extended Kalman filter (EKF) [14] or unscented Kalman filter (UKF) [15]. N i.i.d. samples are then drawn from the GMM representation of the posterior distribution and they are used as a starting point for the next iteration.

The remainder of this section presents the bi-fidelity propagation and an adaptive algorithm for selecting an appropriate number of particles being applied to the EnGMF to reduce its computational cost with an acceptable loss in accuracy. The details of these algorithms are explained in [1].

3.1 Bi-Fidelity Uncertainty Propagation

This research focuses on the use of the bi-fidelity approaches [16, 17] to reduce the computational complexity for the propagation of the EnGMF. The bi-fidelity approach uses both low- and high-fidelity models to reduce computational cost for the propagation of the estimator while maximizing the accuracy of orbit uncertainty propagation.

Likewise to the EnGMF, the process of the bi-fidelity propagation starts from the knowledge of the prior distribution $p(x_{k-1}|y_{k-1})$ which is a multivariate Gaussian distribution with mean $\hat{x}_{k-1|k-1}$ and covariance matrix $P^{xx}_{k-1|k-1}$. For the next step, N i.i.d. samples are drawn from the prior distribution as follows:

$$x_{k-1}(\xi^{(i)}) = \hat{x}_{k-1|k-1} + \left(P^{xx}_{k-1|k-1}\right)^{1/2} \xi^{(i)}, \quad i = 1,2,\cdots,N \tag{24}$$

where $\xi^{(i)}$ denotes the random inputs to the system which follows a standard multivariate normal distribution. A set of low-fidelity samples $x^L(\xi) \in \mathbb{X}$ is then obtained using a low-fidelity propagator. Given a set of random inputs $\Xi = \{\xi^{(i)}\}_{i=1}^N$, the low-fidelity propagated samples can be expressed in the form of matrix as follows:

$$X^L(\Xi) \equiv \left[x^L(\xi^1) \ \cdots \ x^L(\xi^N)\right] \in \mathbb{R}^{n_a \times N} \tag{25}$$

In the case of orbit-state uncertainty propagation, n_a should be increased by considering the state trajectory, i.e., $x^L(\xi)$ should be the state vector $x_0(\xi)$ propagated to the time of interest t using the low-fidelity propagator [9]. The samples then define a subset of $\mathbb{X}$

$$\mathbb{X}^L(\Xi) \equiv \text{span}\left(X^L(\Xi)\right) = \text{span}\left[x^L(\xi^1) \ \cdots \ x^L(\xi^N)\right] \subseteq \mathbb{X}, \tag{26}$$

which is a function of Ξ. The matrix $X^H(\Xi)$ and space $\mathbb{X}^H(\Xi)$ for the high-fidelity samples also has a similar definition. Based on the stochastic collocation method (e.g., see Chapter 20 of [18]), the propagated samples are approximated via the surrogate

$$x^L(\xi) \approx \hat{x}^L(\xi) = \sum_{l=1}^{r} c_l(\xi) x^L(\bar{\xi}^l) \tag{27}$$

where c_l are expansion coefficients, $\bar{\xi}^l$ are the random inputs for the collocation points (or called as important points) in the expansion, and r is the rank of the surrogate with $r \ll N$. The set of the random inputs corresponding to the collocation points, $\bar{\Xi} \equiv \{\bar{\xi}^l\}_{l=1}^r$, is identified using the low-fidelity model. The high-fidelity samples are then approximated as follows:

$$x^H(\xi) \approx \hat{x}^H(\xi) = \sum_{l=1}^{r} c_l(\xi) x^H(\bar{\xi}^l) \tag{28}$$

In brief, in the bi-fidelity approach, the coefficients c_l and the important points $\bar{\xi}^l$ are computed using the low-fidelity samples and this approach includes three assumptions [19]:

- $X^L(\Xi)$ allows for identifying the r samples required for Eq. (28),
- The r high-fidelity samples produce a sufficiently accurate basis for $x^H(\xi) \approx \hat{x}^H(\xi)$, and

- Coefficients c_l of the expansion in Eq. (27) are sufficiently accurate to be leveraged in Eq. (28).

Reference [9] shows through several Earth-orbit test cases that the above three assumptions are reasonable in the context of orbit determination.

The coefficients c_l and important points $\bar{\xi}^l$ are simultaneously calculated in a single algorithm using the following optimization problem:

$$\bar{\Xi} = \arg\min_{\Xi} \inf_{y \in \mathbb{X}^L(\Xi)} \|x^L(\xi) - y\| \tag{29}$$

By solving the optimization problem in Eq. (29), we build a space with basis vectors $x^L(\bar{\xi}^l)$ for $l = 1,\cdots,r$ which minimizes the distance between the points in $X^L(\Xi)$ and the space $\mathbb{X}^L(\bar{\Xi})$; however, it is generally not tractable [17]. A greedy algorithm is therefore used to generate $\bar{\Xi}$ by leveraging a solution to the pivoted Cholesky decomposition and the details of the algorithm are explained in [9] and [17].

3.2 Adapting the Number of Particles

An adaptive algorithm is also used to reduce the computational complexity of the proposed algorithm. It is desirable for the EnGMF to have a small enough covariance matrix such that nonlinear measurement functions can be accurately approximated by linearization in the support of each Gaussian component. In the EnGMF, each component has the same covariance matrix and its magnitude becomes smaller as the number of particles increases, thus the more particles the more accurate the EnGMF performance. This work employs an adaptive algorithm to select an appropriate number of particles and the adaptation rule is based on the convergence assessment method [10].

The adaptive algorithm is based on the predictive PDF of the observations of the EnGMF

$$\begin{aligned} p(y_k|Y_{k-1}^A) &= \int p(y_k|x_k)p(x_k|Y_{k-1}^A)dx_k \\ &\approx \sum_{i=1}^{N} p(y_k|x_k^{(i)})p(x_k^{(i)}|Y_{k-1}^A) \\ &= \frac{1}{N}\sum_{i=1}^{N} n\big(y_k; h_k\big(x_{k|k-1}^{(i)}\big), H_k^{(i)} B_S H_k^{(i)\mathrm{T}} + R_k\big) \end{aligned} \tag{30}$$

where $H_k^{(i)}$ is the Jacobian of the measurement evaluated at the prior mean $x_{k|k-1}^{(i)}$ and Y_{k-1}^A is the collection of all measurement vectors up to and including the current time, $Y_{k-1}^A = y_1,\cdots,y_{k-1}$. It is proven that the approximated predictive observation PDF converges almost surely to the true one as the number of particles tends to infinity [20]. Based on this convergence assessment, an adaptive algorithm for selecting the appropriate number of particles is described below.

The first step is to generate C fictitious observations at each time step k, $\{\tilde{y}_k^{(j)}\}_{j=1}^C$, through Eq. (30). Fictitious observations $\tilde{\boldsymbol{y}}_k^{(j)}$ are generated using the following two steps:

1. Draw C samples $u^{(j)}$ from the discrete uniform distribution $\{1,2,\cdots,N\}$.
2. For each j, draw $\tilde{y}_k^{(j)}$ from the GMM, $\frac{1}{N}\sum_{j=1}^{N} n\big(y_k; h_k(x_{k|k-1}^{(u^{(j)})}), H_k^{(u^{(j)})} B_S H_k^{(u^{(j)})\mathrm{T}} + R_k\big)$.

These sampled fictitious observations are then compared with the actual observation value y_k for the next step. A 1-dimensional observation is assumed here for the sake of simplicity and the same method can be repeatedly applied over each observation element for a multi-dimensional case. The number of the fictitious observations smaller than the actual one is calculated as follows:

$$A_{k,N,C} = \left|\{y \in \{\tilde{\boldsymbol{y}}_k^{(j)}\}_{j=1}^C : y < y_k\}\right| \in \{0,1,\cdots,C\} \tag{31}$$

where $A_{k,N,C}$ is a random variable and $|\cdot|$ represents the number of elements of a set. The value of the random variable $A_{k,N,C}$ indicates the relative position of the actual observation in the fictitious observations. Note that, when the number of particles tends to infinity, the probability mass function (PMF) of $A_{k,N,C}$ almost surely converges to the discrete uniform distribution on $\{0,1,\cdots,C\}$ under mild assumptions [10].

Finally, a chi-squared test [21] is conducted after a set of W consecutive statistics, $S_k = \{a_{k-W+1,N,C}, a_{k-W+2,N,C}, \cdots, a_{k,N,C}\}$, has been obtained from the random variable $A_{k,N,C}$, which is to check whether S_k is a sequence of samples from the uniform distribution on $\{0,1,\cdots,C\}$. The chi-squared statistic is calculated as follows:

$$\chi_k^2 = \sum_{j=1}^{C} \frac{(O_j - E_j)^2}{E_j} \tag{32}$$

where O_j is the frequency of the actual observations being in the j-th relative position in the window size W and E_j is the expected frequency under the null hypothesis, i.e., $E_c = W/(C+1)$. By comparing the p-value associated with the chi-squared statistic $p_{k,C}$ with a preassigned threshold p_l, the number of particles of the EnGMF is adaptively selected. If $p_{k,C}$ is less than or equal to the significance level, we can conclude that the sequence S_k is not sampled from the uniform distribution on $\{0,1,\cdots,C\}$. Therefore, if $p_{k,C} < p_l$, we increase the number of particles to increase the accuracy.

4. NUMERICAL RESULTS

The performance of the GLMB filter with the EnGMF is evaluated through simulations of multi-target tracking problem with sparse observation data. In the simulations, 10 SOs in geosynchronous Earth orbit (GEO) are considered; their initial orbital elements are listed in Table 1. This table shows that some of them are close in the measurement space, which causes many data association hypotheses. The initial uncertainty of each object in Cartesian coordinates is $P_{0,i} = \text{diag}\{10^{-2}, 5\times10^{-2}, 2\times10^{-3}, 5\times10^{-10}, 10^{-9}, 5\times10^{-11}\}$, $i = 1,2,\cdots,10$. The birth and death of targets are not considered in this study. The dynamics model employed here includes the gravitational perturbation due to non-spherical effect of the Earth gravity, the third-body perturbations of the Moon and the Sun, and acceleration perturbation due to solar radiation pressure (SRP). For this study, the EGM2008 [22] gravity model is used for the Earth and 70×70 degrees and order are applied for gravity modeling. We acknowledge that this resolution is higher than necessary for a GEO scenario, but the following timing results should imply a similar improvement in computational efficiency when tracking objects in lower orbits where this gravity model would be more appropriate. The planetary and lunar ephemeris DE430 [23] is selected to calculate the location of the Moon and Sun and the cannonball model is assumed for the acceleration due to SRP. The simulation epoch is 31-December-2014 at 12:00:00 UTC. It is assumed that the shape of each SO is a sphere with a cross-sectional area of 1m^2 and a mass of 100 kg. The coefficient of reflectivity of each SO is set to be 1.5. The system dynamic equations are numerically integrated with an embedded Runge-Kutta 8(7) method [24]. Right ascension, declination, time rate of change of right ascension, and time rate of change of declination measurements are simulated using a ground station located at the top of Haleakala in Maui (latitude = 20.71°, longitude = -156.26°, and altitude = 3.5086 km). Measurements are corrupted by additive zero-mean Gaussian white noise with standard deviations of 0.5 arc-seconds for each angle measurement and 0.05 arc-seconds per second on each angle-rate measurement. Clutter and missed detection are not considered in this study.

Table 1: Initial Keplerian elements for the ten objects

#	Semi-maj. axis (km)	Ecc.	Incl. (deg)	RAAN (deg)	Arg. Periapsis (deg)	Mean Anomaly (deg)
1	42165	0.0003	0.006	81.343	0	91.049
2	42175	0.0003	0.012	81.043	0	91.441
3	42165	0.0003	0.8	80.493	0	89.321
4	42155	0.0003	0.1	81.143	0	90.532
5	42175	0.0003	0.6	81.343	0	91.888
6	42175	0.0003	0.3	98.857	0	91.359
7	42165	0.0014	0.8	99.657	0	89.926
8	42165	0.0003	0.8	99.507	0	89.694
9	42175	0.0006	0.4	98.657	0	91.468
10	42165	0.0014	0.8	80.343	0	89.926

The first goal is to demonstrate and assess the GLMB with the EnGMF ability to handle multi-target tracking problem with short and sparse observation data. The performance of the estimator is evaluated by using a metric called Optimal Sub-Pattern Assignment (OSPA)-on-OSPA, or OSPA$^{(2)}$ [25]. This metric includes localization error as well as

cardinality error. The cut-off, order, and window length are set to be $p = 2$, $c = 1$ km, and $w = 12$. This simulation has one short measurement pass every 12 hours and the measurements are available every 10 seconds with a pass lasting only 2 minutes, i.e., 12 measurements per pass. The tuning parameter h_S for Silverman's rule of thumb of the EnGMF is set to be 1 for long propagation and 0.1 for a short measurement pass. A Monte Carlo analysis is performed with 100 simulations and the EnGMF uses 500 particles in the simulations.

Fig. 1 shows the time history of the Monte Carlo averaged OSPA$^{(2)}$ distance of the GLMB with the EnGMF from the 100 Monte Carlo runs. It is worth nothing that the GLMB with a linear filter for nonlinear systems such as the EKF or the UKF fails (i.e., completely diverges) under this challenging scenario. In the figure, the OSPA$^{(2)}$ distance (blue line) is exactly same as the localization error (red line) and the cardinality error (black line) is zero over time, which means the proposed filter can accurately estimate the number of targets at all times. Moreover, the figure indicates that the proposed filter is able to retain steady state, which means the filter accurately estimates the states of the multiple SOs. The average computation time per filtering run in a C++ implementation on a 3.2 GHz single-core Ubuntu operating system is also evaluated and it is 114.47 seconds for this scenario.

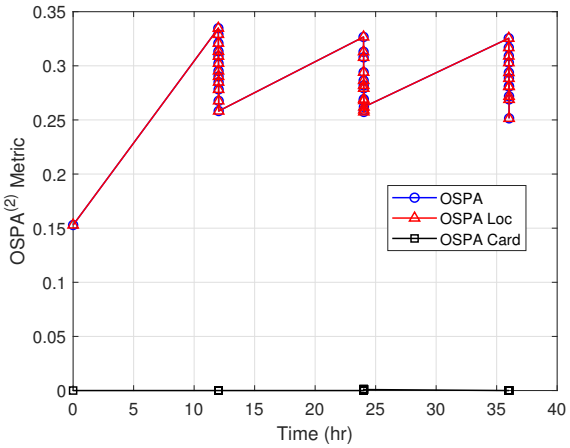

Fig. 1: The OSPA$^{(2)}$ performance for 100 Monte Carlo simulations

In addition, another simulation example under an even sparser observation data condition is used to compare the performances of the GLMB when using: the EnGMF, the EnGMF with bi-fidelity propagation, and the adaptive EnGMF with bi-fidelity propagation. A Monte Carlo analysis is performed with 100 simulations when the gap between measurement passes is increased to 24 hours. In this scenario, the GLMB with the EnGMF with 500 particles diverges in 2 out of 100 simulations. Thus, for the GLMBs with the EnGMF and the EnGMF with bi-fidelity propagation, each target estimator uses 1000 particles, and for the GLMB with the adaptive EnGMF with bi-fidelity propagation, each target first uses 500 particles and if more than two p-values $p_{k,C}$ are below the preassigned threshold p_l then it uses 1000 particles again. The significance level of p-value is set to be 0.15, $p_l = 0.15$. In this scenario, it employs 5 fictitious observations C = 5 and 12 window size W = 12. Likewise the previous simulation, the tuning parameter h_S for Silverman's rule of thumb of the EnGMF is set to be 1 for long propagation and 0.1 for a short measurement pass. The low- and high-fidelity models are summarized in Table 2.

Table 2: Low and high-fidelity dynamic model for the numerical simulations

Dynamic Model	Low-Fidelity	High-Fidelity
Primary Body Gravity	Two body and J_2	70×70
Third-Body Perturbations	None	Sun and Moon
Solar Radiation Pressure	None	Cannonball

Fig. 2 displays the time history of the Monte Carlo averaged OSPA$^{(2)}$ distance of the proposed filters and the average computation time of the 100 simulations, and the averaged OSPA$^{(2)}$ distances are listed in Table 3. The result shows that the GLMB with the EnGMF provides slightly better performance than those of the other two filters in terms of

accuracy; however, comparing to the GLMB with the EnGMF, the GLMB with the EnGMF with bi-fidelity propagation reduces the computation time by 70.70% and the GLMB with the adaptive EnGMF with bi-fidelity propagation reduces the computation time by 82.49%. As a result, it is demonstrated that the GLMB with the EnGMF with bi-fidelity propagation or with the adaptive EnGMF with bi-fidelity propagation can significantly reduce computational time compared to the GLMB with the EnGMF with an acceptable loss in accuracy.

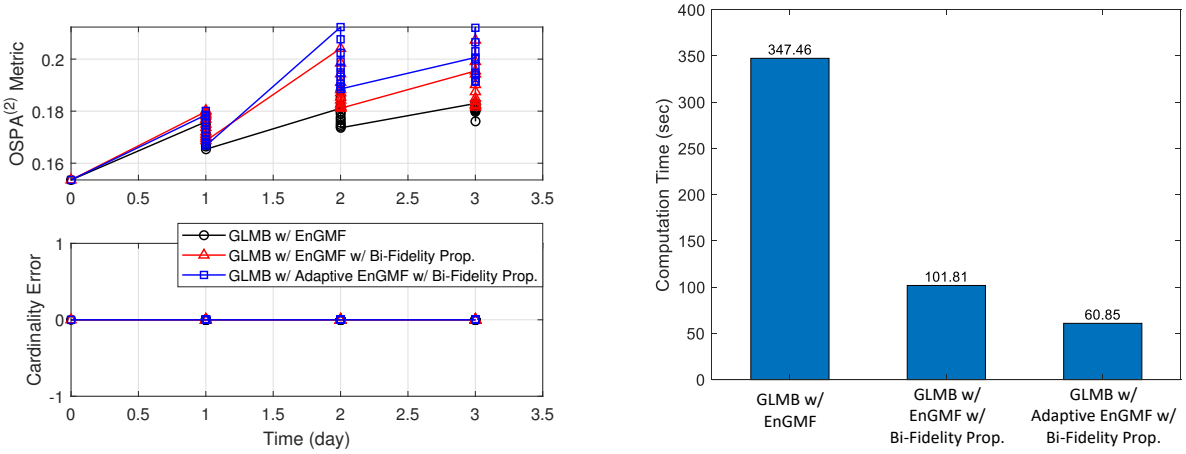

(a) The OSPA$^{(2)}$ performance

(b) The average computation time per filtering run

Fig. 2: The OSPA$^{(2)}$ performance and the average computation time per filtering run for 100 Monte Carlo simulations

Table 3: Averaged OSPA$^{(2)}$ and computation time for 100 simulations

	OSPA$^{(2)}$	Computation time (sec)
GLMB with EnGMF	0.1762	347.46
GLMB with EnGMF with Bi-Fidelity Prop.	0.1832	101.81
GLMB with Adaptive EnGMF with Bi-Fidelity Prop.	0.1880	60.85

5. CONCLUSIONS

The modified kernel-based ensemble Gaussian mixture filtering with the bi-fidelity propagation and an adaptive algorithm is applied to the generalized labeled multi-Bernoulli multi-target tracking filter to track and identify multiple space objects. The performances of the proposed algorithms are analyzed through numerical simulations with a challenging estimation problem of multiple space objects tracking in geosynchronous Earth orbit and it is demonstrated that the proposed filters can accurately estimate targets' states as well as the number of targets. Moreover, it is also shown that the bi-fidelity propagation and the adaptive algorithm can be applied to the baseline algorithm to reduce computational burden with an acceptable loss in accuracy.

6. ACKNOWLEDGMENT

This work was sponsored in part by DARPA (Defense Advanced Research Projects Agency) under STTR contract number 140D0420C0062.

7. REFERENCES

[1] S. Yun, R. Zanetti, and B. A.Jones, "Kernel-based ensemble gaussian mixture filtering for orbit determination with sparse data," *Advances in Space Research*, 2022. doi:10.1016/j.asr.2022.03.041.

[2] B.-T. Vo and B.-N. Vo, "Labeled random finite sets and multi-object conjugate priors," *IEEE Transactions on Signal Processing*, vol. 61, no. 13, pp. 3460–3475, 2013. doi:10.1109/TSP.2013.2259822.
[3] B.-T. Vo, B.-N. Vo, and D. Phung, "Labeled random finite sets and the bayes multi-target tracking filter," *IEEE Transactions on Signal Processing*, vol. 62, no. 24, pp. 6554–6567, 2014. doi:10.1109/TSP.2014.2364014.
[4] M. Arulampalam, S. Maskell, N. Gordon, and T. Clapp, "A tutorial on particle filters for online nonlinear/non-gaussian bayesian tracking," *IEEE Transactions on Signal Processing*, vol. 50, no. 2, pp. 174–188, 2002. doi:10.1109/78.978374.
[5] H. W. Sorenson and D. L. Alspach, "Recursive Bayesian Estimation Using Gaussian Sums," *Automatica*, vol. 7, no. 4, pp. 465–479, 1971. doi:10.1016/0005-1098(71)90097-5.
[6] D. Alspach and H. Sorenson, "Nonlinear bayesian estimation using gaussian sum approximations," *IEEE Transactions on Automatic Control*, vol. 17, no. 4, pp. 439–448, 1972. doi: 10.1109/SAP.1970.270017.
[7] D. W. Scott, *Multivariate Density Estimation: Theory, Practice, and Visualization*. New Jersey, NJ: John Wiley and Sons, 1992. doi:10.1002/0470045345.
[8] B. W. Silverman, *Density Estimation for Statistics and Data Analysis*. London: Chapman and Hall, 1986.
[9] B. A. Jones and R. Weisman, "Multi-fidelity orbit uncertainty propagation," *Acta Astronautica*, vol. 155, pp. 406–417, 2019. doi:10.1016/j.actaastro.2018.10.023.
[10] V. Elvira, J. Miguez, and P. M. Djuric, "Adapting the number of particles in sequential monte carlo methods through an online scheme for convergence assessment," *IEEE Transactions on Signal Processing*, vol. 65, no. 7, pp. 1781–1794, 2017. doi:10.1109/TSP.2016.2637324.
[11] B.-N. Vo, B.-T. Vo, and H. G. Hoang, "An efficient implementation of the generalized labeled multi-Bernoulli filter," *IEEE Transactions on Signal Processing*, vol. 65, no. 8, pp. 1975–1987, 2017. doi:10.1109/TSP.2016.2641392.
[12] B. Liu, B. Ait-El-Fquih, and I. Hoteit, "Efficient kernel-based ensemble gaussian mixture filtering," *Monthly Weather Review*, vol. 144, no. 2, pp. 781–800, 2016. doi:10.1175/MWR-D-14-00292.1.
[13] R. A. Broucke and P. J. Cefola, "On the equinoctial orbit elements," *Celestial Mechanics*, vol. 5, no. 3, pp. 303–310, 1972. doi:10.1007/BF01228432.
[14] A. Gelb, ed., *Applied Optimal Estimation*. Cambridge, MA: The MIT press, 1974.
[15] S. J. Julier and J. K. Uhlmann, "Unscented filtering and nonlinear estimation," *Proceedings of the IEEE*, vol. 92, no. 3, pp. 401–422, 2004. doi:10.1109/JPROC.2003.823141.
[16] A. Narayan, C. Gittelson, and D. Xiu, "A stochastic collocation algorithm with multifidelity models," *SIAM Journal on Scientific Computing*, vol. 36, no. 2, pp. A495–A521, 2014. doi:10.1137/130929461.
[17] X. Zhu, A. Narayan, and D. Xiu, "Computational aspects of stochastic collocation with multifidelity models," *SIAM/ASA Journal on Uncertainty Quantification*, vol. 2, no. 1, pp. 444–463, 2014. doi:10.1137/130949154.
[18] R. G. Ghanem, D. Higdon, and H. Owhadi, *Handbook of Uncertainty Quantification*. Switzerland: Springer International Publishing, 2017.
[19] E. Zucchelli, E. Delande, B. Jones, and M. Jah, "Multi-fidelity orbit uncertainty propagation," *The Journal of the Astronautical Sciences*, vol. 68, pp. 695–727, 2021. doi:10.1007/s40295-021-00267-y.
[20] P. D. Moral, *Feynman-Kac Formulae: Genealogical and Interacting Particle Systems With Applications*. New York, NY, USA: Springer, 2004. doi:10.1007/978-1-4684-9393-1.
[21] R. L. Plackett, "Karl pearson and the chi-squared test," *International Statistical Review*, vol. 51, no. 1, pp. 59–72, 1983. doi:10.2307/1402731.
[22] N. K. Pavlis, S. A. Holmes, S. C. Kenyon, and J. K. Factor, "An Earth gravitational model to degree 2160: EGM2008," in *Proceedings of the European Geosciences Union General Assembly*, (Vienna, Austria), 2008.
[23] W. M. Folkner, J. G. Williams, D. H. Boggs, R. S. Park, and P. Kuchynka, "The planetary and lunar ephemerides DE430 and DE431," IPN Progress Report 42-196, Jet Propulsion Laboratory, California Institute of Technology, http://ipnpr.jpl.nasa.gov/progress_report/42-196/196C.pdf, 2009.
[24] J. R. Dormand and R. J. Prince, "A family of embedded Runge-Kutta formulae," *Journal of Computational and Applied Mathematics*, vol. 6, no. 1, pp. 19–26, 1980.
[25] M. Beard, B. T. Vo, and B.-N. Vo, "OSPA$^{(2)}$: Using the OSPA metric to evaluate multi-target tracking performance," *2017 International Conference on Control, Automation and Information Sciences (ICCAIS)*, 2017. doi:10.1109/ICCAIS.2017.8217598.